Detecting ionizing galaxies with UVEX (WP1)

T. Garel, A. Verhamme & the University of Geneva team

Content

1- Scientific context and objectives

UVEX will perform wide-field deep surveys in the near and far ultraviolet (UV) using broad band imaging (one far-UV and one near-UV band) and a medium resolution spectrometer (Kulkarni et al., 2021). Reaching depths ~50 to 100 times fainter than its predecessor GALEX, the UVEX mission represents a unique opportunity to detect the hydrogen-ionising radiation ($\lambda < 912$ Å restframe), or *Lyman continuum* (LyC), emitted by star-forming galaxies, and quantify the occurrence rate and physical properties of these LyC-leaking sources.

1.1 - Cosmic reionization in the early Universe

Cosmic reionization is one of the most fundamental stages in the history of the Universe, during which the intergalactic medium (IGM) transitioned from a cold, neutral, state to a warm, ionised, phase. In the most favored scenario, energetic ionising radiation leaked by the primordial galaxies in the first gigayear of the Universe is responsible for cosmic reionization. However, direct detections from such distant galaxies ($z > 6$) are impossible due to intervening absorbers in the IGM. We must then resort to nearer sources for which the IGM transmission is least so as to attempt to uncover low-redshift analogs of the sources of reionization.

1.2 - The quest for the analogs of the sources of reionization with UVEX

Over the last decades, very large statistical samples of star-forming galaxies, often identified from their non-ionising stellar continuum emission at ~1500(1+z) Å, have been detected. In contrast, the number of known LyC-leakers remains extremely modest, due to the lack of systematic, deep, UV observing campaigns over large cosmic volumes needed to probe ionising emission. A significant fraction of these known detections come from the Low z Lyman Continuum Survey (LzLCS; Flury et al. 2022), which observed pre-selected LyC candidates with HST. Importantly, LzLCS exclusively targeted LyC leakers at low redshifts ($z<0.4$) and only probed the reddest part of the ionising spectrum at ~900(1+z) Å.

As illustrated in Figure 1 (left panel), UVEX will feature a long-slit spectroscopic bandpass (LSS ; ~1200 to ~3000 Å) and two far-UV and near-UV filters (~1300-1650 Å and ~2000-2850 Å respectively). In principle, it will have access to ionising radiation at 900(1+z) Å from redshifts z~0.3 to z~2.3 (see right panel Figure 1). Shorter wavelengths will also be available with UVEX which may significantly expand the discovery space towards higher redshifts and/or to the blue part of the ionising spectrum of galaxies (i.e. from 400(1+z) to 800(1+z) Å). Note that the Lyα line, which can be instrumental for obtaining accurate redshift measurements, will also be visible up to z ~1.5.

Overall, this highlights that the planned deep wide-field surveys with UVEX have the potential to constrain for the first time the ionising flux properties of the global population of star-forming galaxies over a wide redshift range, and help determine which sub-group is representative of the sources of cosmic reionization.

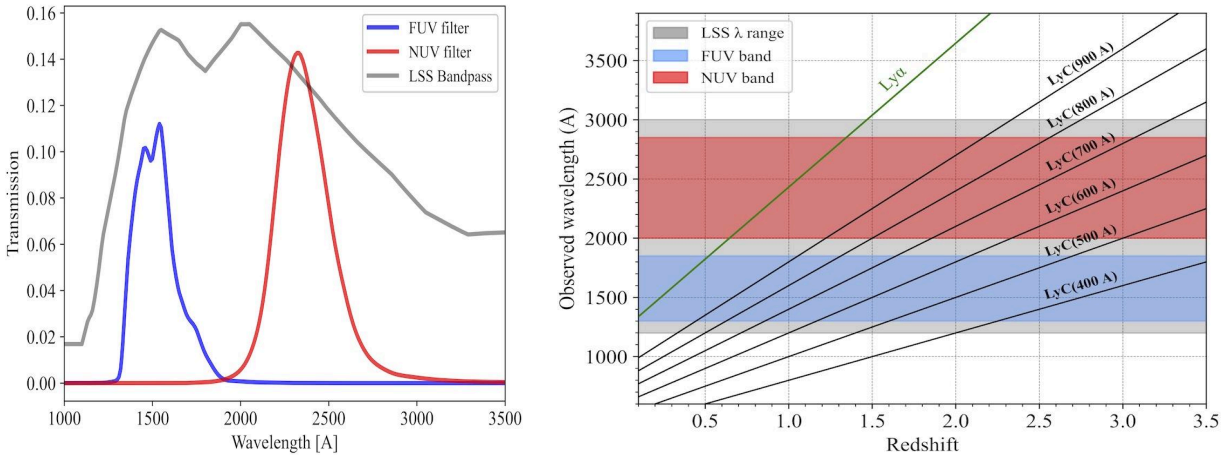

Figure 1. Left: Transmission curves of the far/near-UV filters and long-slit spectrometer bandpass of UVEX. Right: Redshift range of LyC observability with UVEX. The horizontal stripes show the wavelength coverage of the long-slit spectrograph (LSS) and the FUV and NUV bands. Lines depict the wavelengths of the LyC radiation and the Lyα line as a function of redshift.

During its mission, UVEX will likely perform an all-sky survey down to limiting magnitudes m~25-26, as well as targeted observations and spectroscopic follow-ups, for which the exact observational strategy still needs to be refined.

Unless stated otherwise, all quantities presented in this document are in cgs units and use the AB magnitude system and a ΛCDM cosmology (Planck data release 2016).

2- Modelling ionising sources: insights from observations and simulations

2.1 - Observational datasets

As summarised in Table 1, we have compiled LyC observations from four different surveys which span a similar redshift range as UVEX.

Survey	redshift	# LyC detections	rest-frame wavelength [Å]	LyC flux density threshold [erg/s/cm^2/Å]	$L_{1500}/L^*_{z=1}$	reference
LzLCS	*0.2 < z < 0.4*	*50*	*840-890*	*~3.6 x 10^{-18}*	*0.3 - 6*	*Flury et al. 2022, ApJS,260,1F*
AstroSat	*1 < z < 1.1*	*3*	*650-750*	*~6.3 x 10^{-19}*	*0.4 - 1*	*Maulick et al. 2025, ApJ, 984, 40M*
MC22	*3.2 < z < 3.6*	*2*	*830-910*	*~1.6 x 10^{-18}*	*60 - 100*	*Marques-Chaves et al. 2022, MNRAS, 517, 2972*
S18	*2.6 < z < 3.6*	*44*	*880-910*	*~1 x 10^{-20}*	*0.9 - 6*	*Steidel et al., 2018, ApJ, 869, 123*

Table 1. Compilation (non-exhaustive) of observed LyC leakers from the literature.

The LzLCS dataset contains ~50 reliable detections at 0.2<z<0.4, i.e. at the low-redshift end of the UVEX range. We complement our sample with three sources found with AstroSat at z~1, two exceptionally strong LyC leakers at z~3 from Marques-Chavez (2022; hereafter M22) and ~40 objects from the Keck Lyman Continuum Spectroscopic Survey (Steidel et al. 2018; hereafter S18). Measured LyC fluxes are usually between ~10^{-20} and 10^{-16} erg/s/cm^2/Å and are mostly restricted to restframe wavelengths ~700-900 Å.

These observational datasets cover a range of non-ionising UV magnitudes which is typical of the star-forming galaxy population (see Figure 2 and Table 1). The bulk of the sample corresponds to ~$L^*_{z=1}$ galaxies (where $L^*_{z=1}$ is the characteristic UV luminosity at z=1), and extends from ~0.1L* to ~100L*.

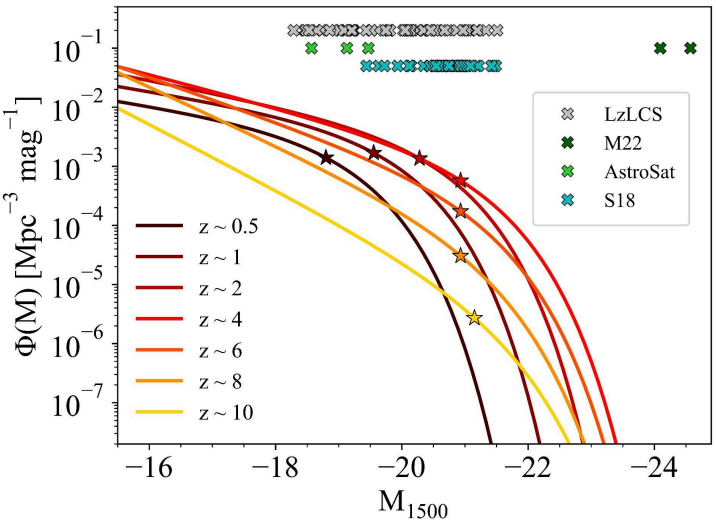

Figure 2. Measured UV luminosity function at 1500 Å restframe from z~0 to 10 (compilation from the literature). The stars mark the characteristic UV luminosities, L, at each redshift. The crosses depict the individual UV magnitudes of the objects in Table 1.*

From the redshift distribution of ionising flux densities of our observational sample (Figure 3), we see that measured ionising fluxes typically decrease with increasing redshift. This is primarily due to flux dilution with cosmological distance, as well as the evolution of IGM opacity.

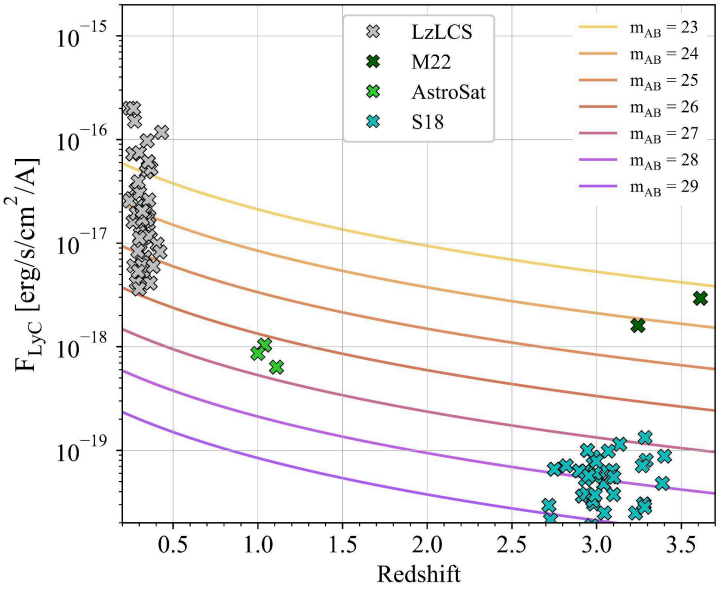

Figure 3. Compilation of LyC detections. This figure shows the flux density of known ionising sources as a function of redshift (see text and Table 1 for details). Colored lines show various levels of apparent magnitudes.

2.2 Simulations of galaxy spectra and intergalactic transmission

The ionising flux density measured at a given observed wavelength λ(1+z) can be expressed as:

$$F_{\lambda(1+z)} = F^{gal}_{900(1+z)} \times (\lambda/900\ A)^{\gamma} \times T_{IGM}(\lambda(1+z)) \quad (1)$$

Here, $F^{gal}_{900(1+z)}$ is the flux density emerging from galaxies at 900 Å restframe. The parameters γ and T_{IGM} correspond respectively to the power-law index characterising the wavelength-dependent shape of the spectrum, and the IGM transmission due intervening hydrogen along the line of sight. We describe in the next sections how these quantities can be predicted using models and simulations.

2.2a - IGM transmission

To model the average IGM transmission T_{IGM} in the redshift range of UVEX, we use the ANAigm model (Inoue et al. 2014). Figure 4 shows that T_{IGM} strongly varies with redshift. At λ=800Å for instance, the transmission decreases from ~90% at z=0.4 to ~10% at z=3.6. At all redshifts, it is also noteworthy that T_{IGM} is significantly higher near the Lyman limit (~912 Å restframe) than at bluer wavelengths. Hence, at fixed survey depth, the expected LyC flux level of a given galaxy is much higher at 900Å compared to e.g. ~300Å (this is –partly– the reason why many ionising detections have been obtained near 900Å). We caution that Helium absorption is not included in ANAigm which may lead to an overestimate of T_{IGM} below ~500Å. Nevertheless, Helium abundance being ~10 times lower than Hydrogen, this effect is most likely sub-dominant.

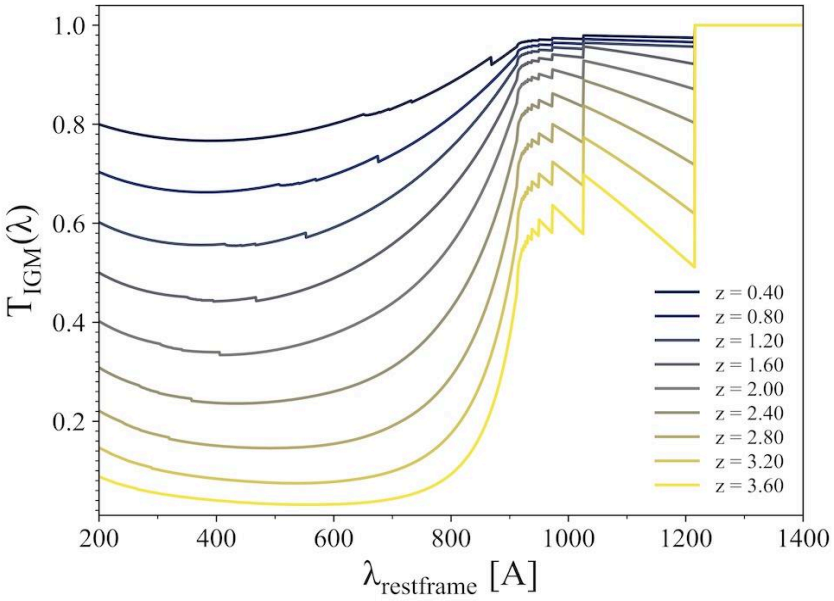

Figure 4. Mean IGM transmission curves as a function of restframe wavelengths for sources at various redshifts (from z=0.4 to z=3.6) computed with ANAigm. It is based on the observed statistics of hydrogen absorbers as a function of redshift and includes both LyC continuum and Lyman series absorptions.

2.2b - Radiation-hydrodynamics simulations

We generate predictions of ionising spectra based on simulations of a star-forming galaxy undergoing a starburst phase presented in Mauerhofer et al. (2021). This zoom-in simulation features fully coupled radiation-hydrodynamics which allows for realistic forward modelling of observable galactic properties. It has been run with the RAMSES-RT code using state-of-the-art subgrid models of baryonic physics to compute gas cooling, star formation, supernova feedback, etc. It has been post-processed with the RASCAS radiative transfer code to produce mock observations along 1728 different directions. The simulated spectra are based on the BPASS v2.1 stellar synthesis models with a Kroupa IMF (Stanway & Eldridge 2018) and only include the radiation transport within the interstellar medium (not the effect of IGM) so as to predict the fraction of escaping photons. Importantly, this simulation has been shown to successfully reproduce various observational constraints such as the diversity of UV line profiles (Blaizot et al. 2023, Gazagnes et al. 2024), quantities that are directly connected to the production and escape of ionising photons from galaxies. The simulated galaxy exhibits UV magnitudes between M_{1500}~17.5 to -19.5 (depending on the direction of observation) which corresponds to ~0.1-1L* at z=1.

LyC spectral shapes

Figure 5 shows examples of simulated LyC spectra measured along different sightlines. Ionising emission extends from the Lyman limit at 912 Å down to ~300 Å restframe and then quickly drops to zero at shorter wavelengths. This figure highlights the significant scatter from one sightline to another in terms of ionising flux level and spectral shape. As illustrated by Figure 6, the ionising power-law indexes γ of the simulated spectra vary from nearly flat (γ~0) to very steep (γ~-3) shapes, with a mean value around -0.7.

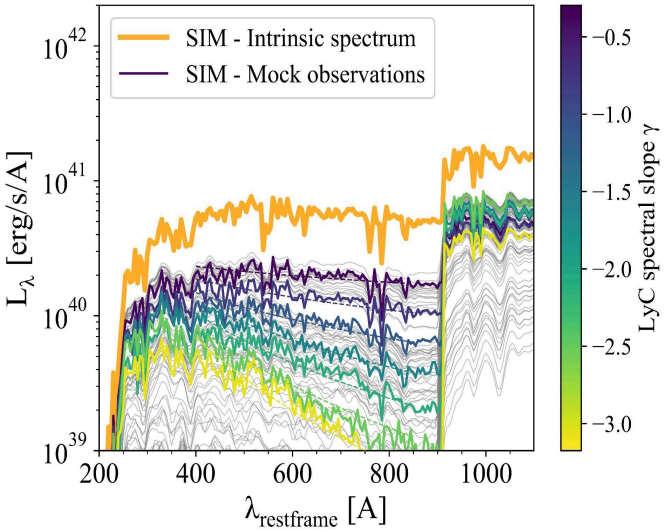

Figure 5. Simulated LyC spectra. The thick orange line shows the isotropic intrinsic emission produced by stars within the galaxy while thin grey lines represent the spectra seen along various directions after radiative transfer in the ISM. Yellow-to-blue colored lines emphasize ionising spectra with different slopes γ.

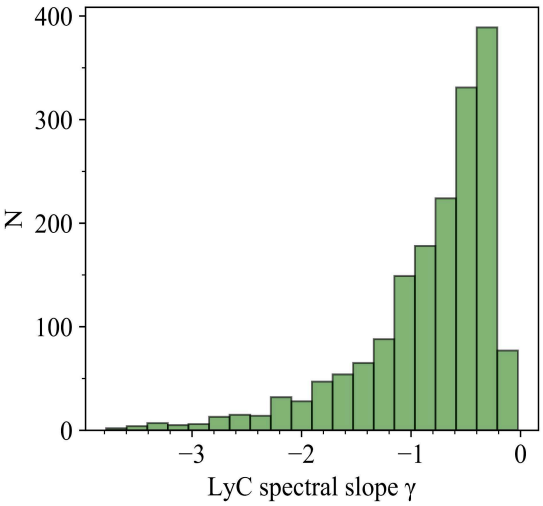

Figure 6. Distribution of best-fitting spectral slopes γ of the simulated LyC spectra.

Ionising to non-ionising flux ratio

The ionising to non-ionising flux ratio R, typically measured at 900Å versus 1500Å restframe, is often used to characterise the LyC leakage in star-forming galaxies. It can notably be used as a reasonably accurate proxy for the escape fraction of ionising radiation (e.g. Flury et al. 2022). The R values inferred from our observed and simulated datasets span a rather similar range (from ~ -3 to 0 in log$R$; see Figure 7), although observational measurements are restricted to slightly higher values (log$R \gtrsim$ -2). This is probably an observational bias owing to the detection limits inherent to any galaxy survey. These predicted flux ratios, R, will be instrumental in Section 3 for estimating the ionising fluxes from non-ionising fluxes in mock galaxy populations.

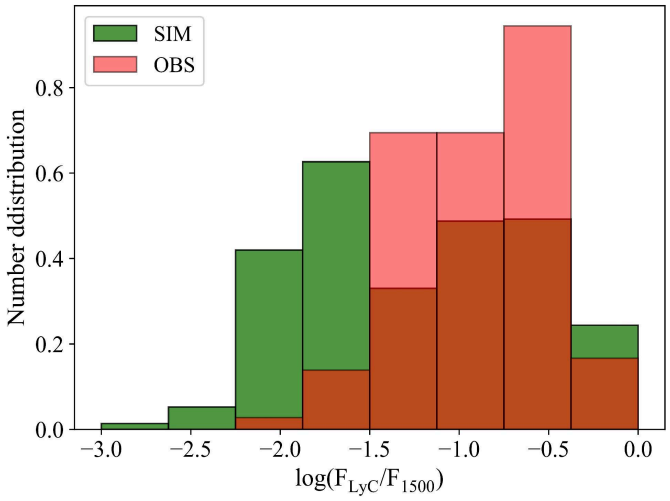

Figure 7. Distribution of ionising to non-ionising flux ratio $R = F_{900} / F_{1500}$ for our observational (pink) and simulated (green) datasets. Observational ratios are the measured values (i.e. uncorrected for IGM attenuation) while simulated ratios are intrinsic R values, i.e. before IGM attenuation.

3- Number counts forecast for UVEX

The existing samples of known individual LyC detections (see Table 1) are quite heterogeneous and incomplete, and no survey of LyC leakers with a well-defined selection function has ever been carried out successfully. Thus, predicting accurately the occurrence rate and number counts of these objects among the underlying galaxy population is highly challenging. Nevertheless, we can attempt to provide quantitative forecasts using the modelling presented in Section 2.2 and mock lightcones generated with simulated cosmological data cubes (see below).

3.1 Mock galaxy catalogs

We generate mock galaxy catalogs with the Theoretical Astronomical Observatory (TAO) by constructing custom "lightcones" from semi-analytic models based on cosmological simulations. In practice, we build unique lightcones of 1 square degree from z=0.3 to 3.5 using the SAGE semi-analytic model of galaxy formation (Croton et al., 2016) and the Bolshoi-Planck N-body simulation (Rodríguez-Puebla et al., 2016). We use an empirical dust attenuation model to calibrate SAGE on the observed UV luminosity functions from z~0 to 3 in order to predict the right number density of galaxies at a given magnitude M_{1500} at each redshift (Figure 8). Each lightcone thus provides statistical galaxy samples with known redshift, position, and dust-attenuated UV flux/magnitude at 1500Å restframe.

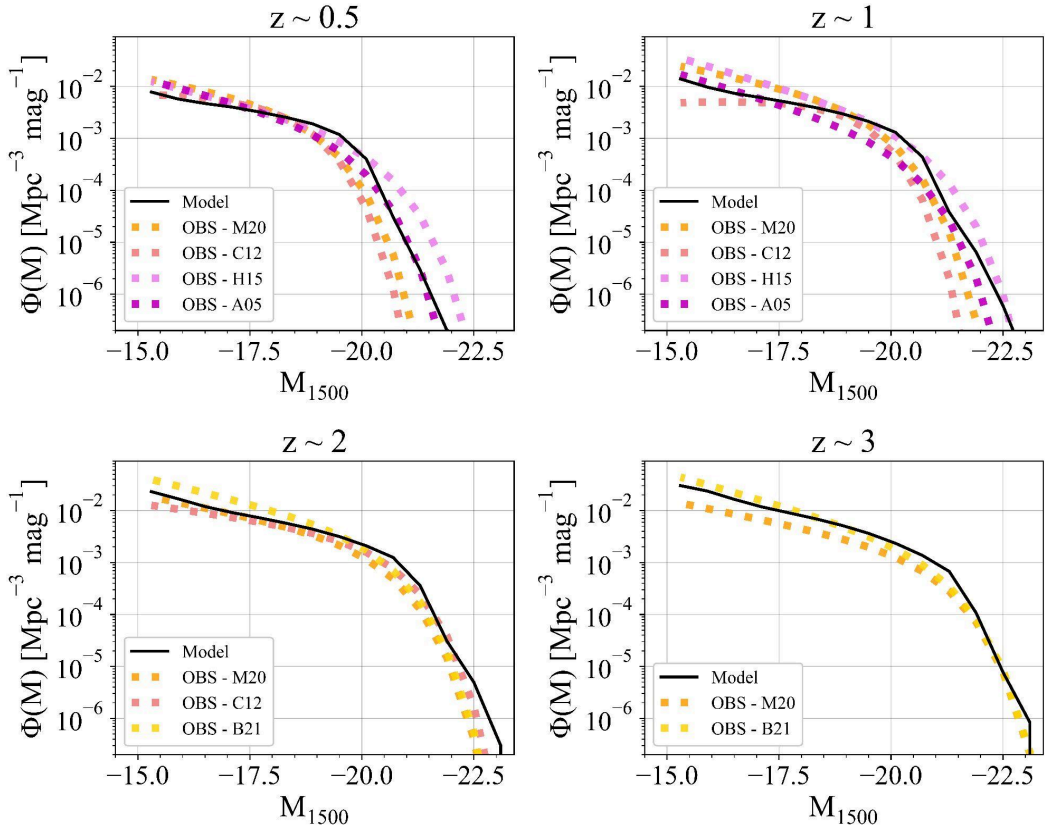

Figure 8. UV luminosity functions at 1500Å restframe from the SAGE model (black solid lines) calibrated against observational constraints (colored dotted lines).

3.2 Ionising emission of mock galaxies

Three of the main critical parameters to estimate the detectability of typical LyC leakers are the IGM transmission (T_{IGM}), the slope of the LyC spectrum (γ) and the ionising to non-ionising flux ratio (R). The distribution of R values presented in Section 2.2 was obtained from known observational detections and a starburst galaxy simulation, hence it is unavoidably biased towards galaxies experiencing a LyC-bright phase. Indeed, the LyC emissivity of galaxies mostly originates from short-lived massive stars during starbursts (~10 Myr timescale) whereas stellar emission radiated at 1500 Å is rather steadily tracing star formation over longer timescales (~100 Myr). The starburst phase is thus subject to a "duty cycle" so one can make the hypothesis that only a fraction of galaxies are emitting ionising radiation at a given time.

Thus, we adopt the starburst fraction f_{SB} as an additional parameter to account for this duty cycle. Taking f_{SB} = ~10 Myr / ~100 Myr = 0.1, we set the LyC emission to zero for a fraction (1-f_{SB}) of our mock galaxies. The ionising spectrum of the rest of the mock galaxies (i.e. those assumed to be in a starburst phase) is estimated similarly to Eq. (1) using the predicted IGM transmission, ionising spectral shape γ, and flux ratio R presented in Section 2.2 such that :

$$F_{\lambda(1+z)} = R \times F_{1500(1+z)} \times (\lambda/900\,A)^{\gamma} \times T_{IGM}(\lambda(1+z)) \quad \text{for starbursts} \qquad (2)$$
$$F_{\lambda(1+z)} = 0 \quad \text{for non-starbursts}$$

where $F_{\lambda(1+z)}$ is the observed LyC flux density (computed between 300 and 912 Å restframe). For each galaxy, γ and R are randomly drawn from the distributions in Figure in 6 and 7. Overall, we generate 1,000 catalogs accounting for both the random sampling of the duty cycle of starburst galaxies and the field-to-field variation in the different mock lightcones.

3.3 Expected number counts

3.3a Spectroscopic number counts

Figure 9 presents the predicted UVEX number counts per square degree as a function of the LyC flux density evaluated at three different (restframe) wavelengths – 900, 700 and 500 Å. Colored lines show the expected values per redshift bin whereas black curves correspond to the total number counts. At 900(1+z)Å, we predict nearly 30 objects per sq. degree at F>10^{-17} erg/s/cm²/Å, most of them sitting at the low redshift end (z<0.6). A few detections per sq. degree are also expected at the same flux level for bluer wavelengths, though at higher redshifts, i.e. z~0.6-1 and z~1.2-1.8 at 700(1+z) and 500(1+z)Å respectively.

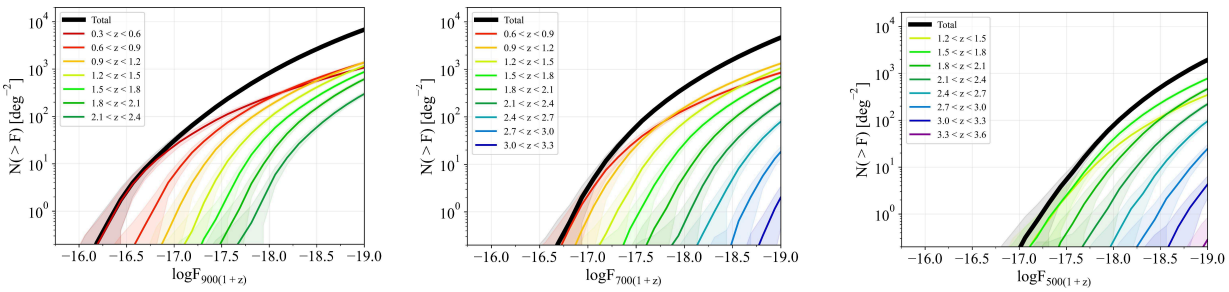

Figure 9. Predicted (cumulative) number counts per square degree in terms of LyC flux density at observed wavelengths λ_{obs} = 900, 700 and 500 x (1+z) Å based on the mock lightcones. Only galaxies with λ_{obs} falling in the

spectral range of UVEX's LSS have been considered in each panel. The thick black line shows the total numbers from z=0.3 to z=3.6 whereas thin colored lines show the forecasts per redshift interval. Shaded regions show the dispersion due to the random sampling of starburst galaxies and the field-to-field variation.

The redshift distributions in Figure 11 highlight the most favorable redshift range for specific parts of the LyC spectrum. Emission at 900(1+z)Å can be efficiently probed at z~0.4-1 while detections at shorter restframe wavelengths (e.g. 500(1+z)Å) are most likely around z~1.5.

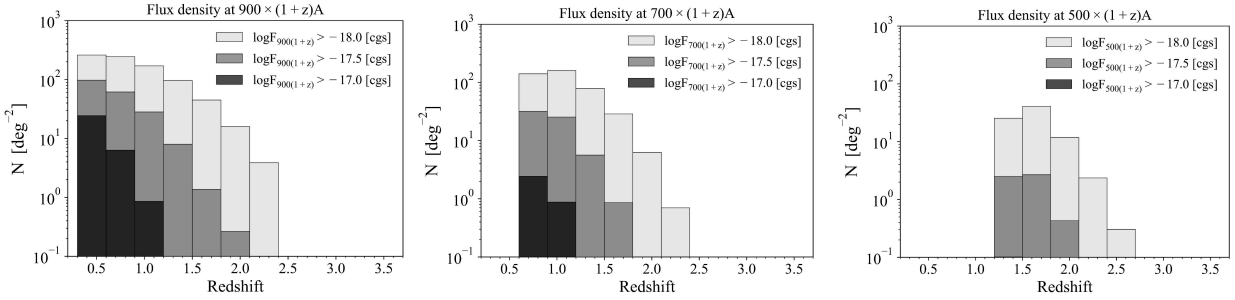

Figure 11. Predicted redshift distributions of LyC spectroscopic detections for various flux detection limits : F_{LyC} > 10^{-17}, $3x10^{-17}$ and 10^{-18} erg/s/cm^2/Å. The three panels correspond to the LyC flux densities measured at 900, 700 and 500 x (1+z) Å.

Overall, the requirement for direct LyC spectroscopic identifications (≳ 10/deg^2) at z ≲ 1 is approximately 10^{-17} erg/s/cm^2/Å. Extending the detection limit down to ~10^{-18} erg/s/cm^2/Å would significantly increase the statistics by a factor 50 (see Table 2 at the end of this document) and help uncover sources at z >1.5 and/or probe bluer parts of the spectrum. The aforementioned flux limits are likely achievable in some deep UVEX surveys according to the UVEX Science Implementation document (their Table E-2). Except for potential ultra-bright sources, spectroscopic detections at redshifts greater than ~2 seems however compromised, unless the UVEX mission carries out much deeper exposures in some targeted field observations.

3.3a Photometric number counts

The same methodology is used to provide estimates of apparent magnitudes in the FUV and NUV bands by convolving our mock ionising spectra with UVEX filters (Figure 1 left).

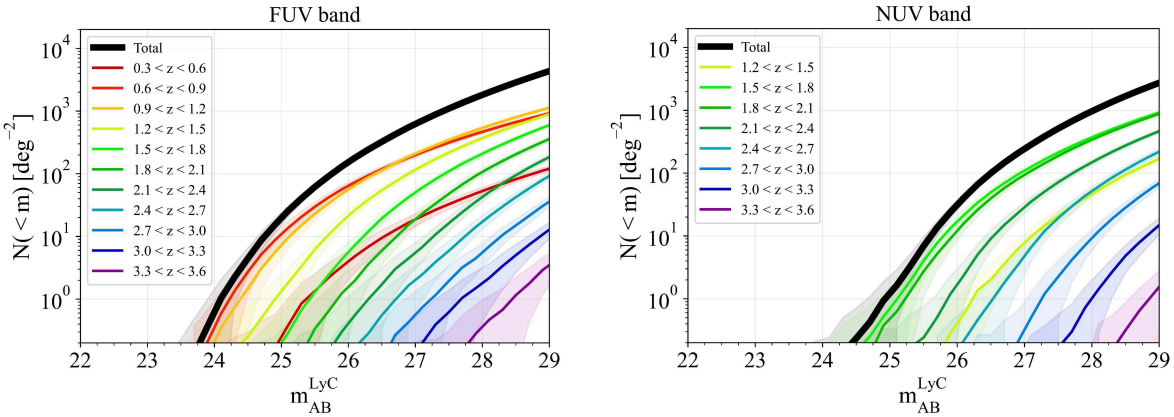

Figure 10. Predicted (cumulative) number counts per square degree in the FUV (left) and NUV (right) bands based on the mock lightcones. Apparent magnitudes are computed using the modelled ionising spectra of LyC-emitting galaxies.

The non-ionising flux (λ>912 Å) is assumed to be zero. The thick black line shows the total numbers from z=0.3 to z=3.6 whereas thin colored lines show the forecasts per redshift interval. Shaded regions show the dispersion due to the random sampling of starburst galaxies and the field-to-field variation.

UVEX's FUV band should be much more efficient than the NUV band at probing LyC leakers, as illustrated by Figure 10. At m_{AB} < 25 (<26), ~20 (~200) sources per sq. degree should be bright enough to be seen in the FUV. While the bulk of the detections should arise from 0.5 < z < 1.2, we expect ~1 object per sq. degree at m_{AB}<26 at z~2. In the NUV, ~1 (~30) candidates per sq. degree are predicted at m_{AB}<25 (<26), most of them falling in the redshift range 1.5< z < 2.5.

We caution that only the ionising part of the stellar spectra has been modeled to compute the magnitudes presented here, i.e. non-ionising flux has been set to zero. In practice, UVEX filters are broad enough such that radiation at λ > 912 Å shall nearly always contribute to the photometry. Disentangling ionising and non-ionising components from imaging only is quite challenging and surely requires additional constraints, such as e.g. the accurate knowledge of the spectral shape of the SEDs and precise systemic redshift measurements. Ancillary data and/or UVEX spectroscopy may be crucial to correctly identify genuine LyC leakage from the photometric candidates.

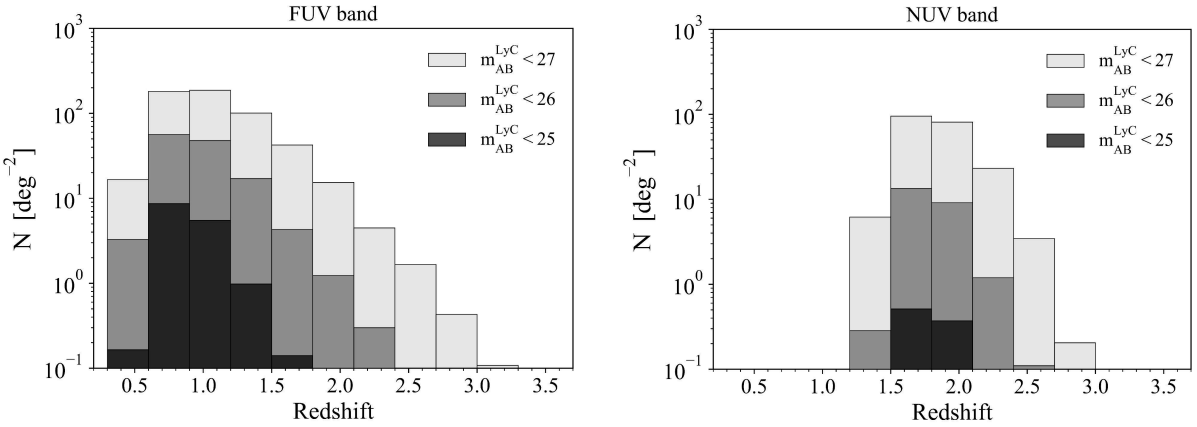

Figure 12. Predicted redshift distributions of LyC apparent magnitudes in the FUV (left) and NUV (right) bands for different detection limits : m_{AB} *< 25, 26 and 27.*

The redshift range z=0.5-1.2 appears to be the "sweet spot" for LyC candidate detections with UVEX (see Figure 12), owing to a trade-off between flux dilution with redshift and the wavelength coverage of the FUV filter. Similarly, brightest sources (m_{AB}*<25) in the NUV band are expected at z=1.5-2. We note that pushing down to* m_{AB}*~26-27 may increase the number of objects by one or two orders of magnitude and help uncover many more candidates at higher redshifts (see Table 3 below).*

SUMMARY

Deep wide-field surveys targeting the extreme/far restframe UV hold enormous potential to identify statistical, representative, samples of ionising galaxies that are analogs to the sources of cosmic reionization. Such observations will provide unique and robust constraints on the occurrence rate of LyC leakers, the ionising escape fraction and spectrum shape of star-forming galaxies, as well as their evolution with redshift and galaxy properties.

Using observational and simulation-motivated arguments to predict the transmission of the intergalactic medium and the ionising emission properties of galaxies, we have generated mock catalogs based on cosmological simulations to provide forecasts for UVEX-like surveys. To date, the fraction of star-forming galaxies being in a LyC-emitting phase remains completely unknown and it is one the most critical parameters that needs to be constrained by forthcoming observational campaigns. In this study, a fraction of 10% has been adopted in order to estimate the number counts per square-degree and associated variance (as summarised in Table 2 and 3).

	F_{lim} = 10^{-17}		F_{lim} = 5x10^{-17}		F_{lim} = 10^{-18}	
wavelength	<N>	std dev	<N>	std dev	<N>	std dev
900 Å	32	+/- 6	197	+/- 15	836	+/- 33
700 Å	4	+/- 2	64	+/- 9	414	+/- 24
500 Å	0.2	+/- 0.4	6	+/- 2	81	+/- 10

Table 2. Global number counts per square degree over the full redshift range of the LSS ($0.3 \leq z \leq 3.6$) estimated at different restframe wavelengths (λ=900, 700 and 500Å restframe) for various flux density limits (in erg/s/cm^2/Å). <N> is the mean number per square degree and stddev is the standard deviation estimated from the 1000 mock catalogs.

	m_{lim} = 25		m_{lim} = 26		m_{lim} = 27	
band	<N>	std dev	<N>	std dev	<N>	std dev
FUV	15	+/- 4	130	+/- 12	552	+/- 29
NUV	1	+/- 1	24	+/- 5	208	+/- 17

Table 3. Global number counts per square degree in the FUV and NUV bands for various limiting magnitudes. <N> is the mean number per square degree and stddev is the standard deviation estimated from the 1000 mock catalogs.

Thanks to its wide spectral coverage (~1200-3000 Å), UVEX will provide unique spectroscopic and photometric measurements of the ionising spectrum of galaxies in the redshift range z~0.5-3 down to very blue restframe wavelengths (~400Å). Our study suggests that as much as ~15-35 objects/deg^2 have typical LyC flux densities and LyC magnitudes brighter than F=10^{-17} erg/s/cm^2/Å and m_{AB}=25 respectively. The bulk of the candidates sits in the 'LyC redshift desert' at z=[0.5-1.5], hence filling the gap between known LyC samples at z<0.3 and z=2-3. Pushing down to F=10^{-18} erg/s/cm^2/Å and m_{AB}=27 increases the number counts per square degree by a factor ~50 and reduces the associated uncertainty by a factor ~5 (note that the contribution of cosmic

variance to the total variance is likely underestimated because of the limited size of our mock lightcones, i.e. 1 deg^2).

Assuming a long-slit of 2°x10'', the predicted number of ionising spectroscopic measurements in an "all-sky" survey (e.g. 15,000 deg^2) is about 3,000 at $F=10^{-17}$ $erg/s/cm^2/Å$. UVEX's broad band imaging will also be extremely powerful at detecting LyC-leaker candidates, provided that the respective contributions of ionising and non-ionising emissions falling into the band can be disentangled (e.g. using UVEX's spectrograph and/or ancillary data). Our modelling predicts that the FUV band will be the most efficient at probing ionising sources, mainly around z~0.5-1.2. At $m_{AB}=25$, we expect ~200 candidates per pointing (i.e. in a field-of-view of 3.5°x3.5°) and as many as ~240,000 over 15,000 deg^2.

References

Arnouts, S., Schiminovich, D., Ilbert, O., et al. 2005, ApJL, 619, L43

Blaizot, J., Garel, T., Verhamme, A., et al. 2023, MNRAS, 523, 3749

Croton, D. J., Stevens, A. R. H., Tonini, C., et al. 2016, ApJS, 222, 22

Cucciati, O., Tresse, L., Ilbert, O., et al. 2012, A&A, 539, A31

Flury, S. R., Jaskot, A. E., Ferguson, H. C., et al. 2022, ApJS, 260, 1

Gazagnes S. et al., 2024, ApJ, 969, 50

Inoue A. K., Shimizu I., Iwata I., Tanaka M., 2014, MNRAS, 442, 1805

Kulkarni, S. R., Harrison, F. A., Grefenstette, B. W., et al. 2021, arXiv:2111.15608

Marques-Chaves et al. 2022, MNRAS, 517, 2972

Maulick et al. 2025, ApJ, 984, 40M

Mauerhofer V., Verhamme A., Blaizot J., Garel T., et al., 2021, A&A, 646, A80

Moutard, T., Sawicki, M., Arnouts, S., et al. 2020, MNRAS, 494, 1894

Rodriguez-Puebla A., Behroozi P., Primack J., Klypin A., Lee C., Hellinger D., 2016, MNRAS, 462, 893

Stanway E. R., Eldridge J. J., 2018, MNRAS, 479, 75

Steidel et al., 2018, ApJ, 869, 123